J Mater Sci (2009) 44:64–73
DOI 10.1007/s10853-008-3115-y

Phase selection in supercooled Cu–Nb alloys

A. Munitz · M. Bamberger · A. Venkert · P. Landau · R. Abbaschian

Received: 18 June 2008 / Accepted: 12 November 2008 / Published online: 20 December 2008

Abstract Electromagnetic levitation was used to determine Cu–Nb phase diagram and to study supercooling effects on solidification characteristics of the alloys containing 5–70 wt% Nb. The Cu–Nb stable phase diagram was found to exhibit near-flat liquidus with a peritectic reaction at 1093 °C. Melt separation was found only for specimens containing approximately 20 wt% Nb. The results indicate that melt separation in the alloy requires supercooling exceeding 230 K combined with high cooling rates during solidification. Some specimens quenched from the solid + liquid zone on a copper chill also show evidence of melt separation which is attributed to minor oxygen impurities. Nb-rich liquid which nucleates below the T_0 curve solidifies as a metastable Nb-bcc lattice containing only 67 wt% Nb as compared to 96 wt% of the regular Nb dendrites.

A. Munitz (✉) · A. Venkert
Nuclear Research Center-Negev, P.O. Box 9001, Beer-Sheva, Israel
e-mail: munitza@yahoo.com

M. Bamberger
Materials Science and Engineering, Technion, Technion City, Haifa, Israel

P. Landau
Materials Science and Engineering, Ben-Gurion University, Beer-Sheva, Israel

R. Abbaschian
College of Engineering, University of California, Riverside, CA 92521, USA

Introduction

Copper–niobium alloys have gained interest due to their high superconductivity [1, 2] and improved mechanical properties [3, 4]. In both aspects, the stable and metastable phases are extremely important for understanding and predicting the microstructure. However, until recently, two-phase diagrams of the Cu–Nb were proposed in the literature. Popov and Shiryaeva [5] suggested a phase diagram which indicate a liquid state immiscibility with a monotectic reaction. On the other hand, Allibert et al. [6] indicates horizontal liquidus but no immiscibility. Recently, Smith et al. [7] concluded, that stable phase diagram of Cu–Nb should have nearly horizontal liquidus with a peritectic reaction, a conclusion similar to that of Chakrabarti and Laughlin [8]. This near plateau is indicative of a possible metastable miscibility gap. However, melt separation has so far been found only in alloys containing minor additions of oxygen in the melt [2].

The Cu–Co and Cu–Fe exhibit a definite thermodynamic tendency for liquid immiscibility upon supercooling, as evidenced by nearly flat liquidus curves and positive deviation of their activities from Raoult's Law [9]. The present authors investigated the Cu–Co [10, 11], Cu–Fe [9], and Cu–Co–Fe [12, 13] systems using the levitation technique, and indeed found a metastable liquid miscibility gap. No such observation has been made for the Cu–Nb system. The difficulty in investigating Nb alloys is due to the high temperature required for processing. Electromagnetic levitation [9, 10, 14] is a technique in which these alloys can be investigated. It has the advantage of reducing contamination and heterogeneous nucleation, as well as enhancing melt homogeneity and allowing for relatively easy temperature measurement, and atmosphere control.

The major goal of this study work was to provide additional details on the effects of supercooling on the microstructure and melt separation of Cu–Nb alloys using the electromagnetic levitation technique.

Experimental procedures

Specimen preparation

Copper and niobium (99.99% pure) samples, weighing approximately 1.5 g, were alloyed by arc melting in an Ar environment using a non-consumable tungsten electrode. For each arc melted sample, the individual alloy components were weighed, with an accuracy of ±0.01 g, according to the desired bulk composition listed in Table 1. The arc-melting period was kept relatively brief, normally a few seconds, to allow for melting of Cu and formation of a single button. Each arc-melted button was then levitated and processed using the electromagnetic (EM) levitation apparatus. The experimental procedure for EM levitation is described elsewhere in detail [10, 15, 16]. It involved levitation of approximately 1.5 g samples in a glass tube, through which a stream of Ar or He + Ar mixture was passed to prevent sample oxidation and control its temperature. The He and Ar were passed through a gas purifier containing a titanium receiver at 800 °C to minimize oxygen impurity content. The arc-melted specimens were lowered into the levitation coil, with Ar flowing around the sample. The sample was heated by adjusting the levitation power or reducing the gas flow rate until it melted and superheated about 100 K. The sample was then cooled by increasing the He flow until nucleation and recalescence were attained. After nucleation, the He flow was reduced to melt the sample again, if so desired. The cooling and heating cycles were repeated several times to determine the liquidus temperature of the specimen and to record the maximum supercooling attainable. Finally, when the liquid attained a desired value of supercooling (or superheating), the levitation power was cut off, allowing the specimen to quench onto a coper plate. Some samples were solidified while levitated at cooling rates of around 100–200 K/s, others were quenched on a copper chill, from a starting drop temperature T_{drop}. Starting states could be either a superheated liquid, a solid/liquid mixture, or a supercooled liquid. The temperature of the levitated specimens was continuously monitored using a two-color optical pyrometer equipped with a data acquisition system.

Table 1 Summary of specimen compositions used in this study, and the melting temperatures obtained in comparison with literature data

Alloy composition (wt% Nb)	Supercooling obtained (K)	Melting temperature		
		This study		Literature [22] (°C)
		Experimental (°C)	Calculated (°C)	
5	170	1510	1500	1380
8.1				1520
10	210	1540	1620	
12.0				1596
15				1658
20	270	1550	1700	
21.6				1668
26.0				1670
30	250	1580	1710	
35.0				1675
40	300	1645	1730	1688
50		1665	1730	1718
55.5				1728
60	100	1705	1730	
68.6				1765
70		1925	1770	
86.0				1848

The thermal history of a Cu-40 wt% Nb sample is illustrated in Fig. 1. The first sharp deflection of the curve in the first cycle presents the melting temperature of the copper. At about 1400 °C (point "a") a second deflection is observed, which represents the massive Nb dissolution in the molten copper. Further heating causes a monotonic temperature increase until the entire Nb is dissolved. At this point (point "b") a third deflection is observed, which represents superheating of the liquid. When the temperature reached a desired level, usually around 100 K above the liquidus temperature, the cooling He gas was introduced allowing the sample temperature to decrease. This process was repeated cyclically. During some cooling cycles, melt supercooling was observed as noted by T_R in Fig. 1. To minimize copper evaporation, alloys having a high Nb concentration were kept for only a very short time in the liquid state. At a certain point, the cooling gas was shut down, and the second cycle began. Usually, during the first 2–3 cycles the alloy is homogenized and all the surface

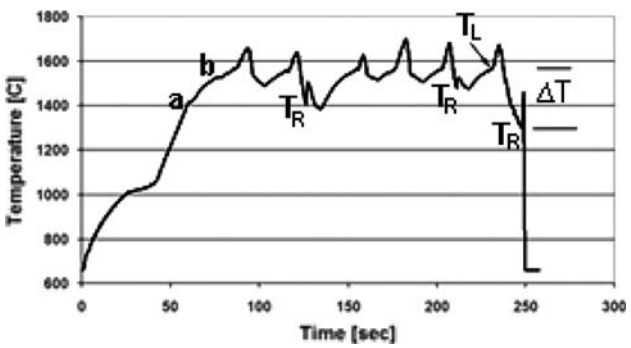

Fig. 1 Thermal history of Cu-40 wt% Nb specimen

contamination is evaporated thus allowing the melt to supercool. Upon nucleation recalescence occurs, which is designated by T_R. At this point, a sharp exothermal reaction occurs (accompanied by a sudden increase in the sample brightness) and the sample temperature increases rapidly. For the sample shown in Fig. 1, recalescence is observed in the second, fifth, and the last cycle when a supercooling of about 270 K was obtained. Table 1 shows a summary of measured melting temperatures, together with those calculated in this study as discussed in Section Thermodynamic calculations, as well as the values published in literature [17].

Microstructural characterization

The specimens were cross-sectioned, polished, and subsequently etched for 2–3 s at room temperature using a solution of 10 g $CuCl_2$ and NH_4OH sufficient for dissolving all the cupric chloride crystals in 120 mL of distilled water. For energy dispersive spectroscopy (EDS) analysis, the specimens were etched lightly to reveal the microstructure while keeping the surface roughness to a minimum. The EDS composition data were corrected using EDS equipped with a standard ZAF program. In order to confirm the accuracy of the EDS results, several specimens were also checked using wavelength dispersive spectroscopy (WDS), using pure Cu, and pure Nb as standards. The two measurement techniques were found to agree by better than 0.3 wt%.

Transmission electron microscopy

For transmission electron microscopy, about 150-μm thick slices were cut from the samples using an electro-erosion machine, from which 3-mm diameter disks were punched out. Final thinning was achieved by mechanical grinding followed by ion milling in a Gatan PIPS© (Precision Ion Polishing System). Transmission electron microscopy was carried out on a JEOL 2010 electron microscope with energy dispersive X-ray capabilities.

Thermodynamic calculations

Thermodynamic calculation of the binary Cu–Nb diagram were performed on the basis of the Gibbs free energy for the pure elements and for the phases present in the alloy system. The calculations used the ThermoCalc software and published thermochemical and equilibrium data for the addressed binary system [18]. The coexisting metastable phases in the supercooled melt were calculated using the same database, by suppressing the Cu-fcc and Nb-bcc solid phases.

Results

Secondary electron (SE) images illustrating the microstructure of Cu–Nb alloys dropped from the solid + liquid (S + L) region as a function of Nb concentration are shown in Fig. 2. For Cu-5 wt% Nb shown in Fig. 2a, the primary Nb dendrites are surrounded by a Cu-rich phase. In Fig. 2b–d, coarse and fine Nb dendrites are revealed. The coarse dendrites in Fig. 2b–d are Nb primary dendrites solidified while levitating, whereas the finer dendrites formed on solidification of the solid + liquid on the copper chill. As can be seen, the solidified finer dendrites surround the coarse dendrites. The density and the size of the coarse dendrites increased with Nb concentration in the melt. Elemental microanalysis of the Cu and Nb in the coarse and fine dendrites show that the Nb concentration of the dendrites ranges between 95.2 and 96.3 wt%.

The interdendritic regions microstructure as a function of the Nb concentration in the melt is presented in Fig. 3. The interdendritic region for specimens of low Nb concentrations (up to 10 wt%) contained a cell structure (Fig. 3b) with two zones: a dark interior section surrounded by a region imaged lighter. Elemental microanalysis of the Cu and Nb in these cells show that the Nb concentrations in the center and the circumference are 3.9 and 0.8 wt%, respectively. For alloys with Nb concentration above 10 wt%, the interdendritic region morphology changed from a cell structure (Fig. 3b) to the ones shown in Fig. 3c and d.

Secondary electron Images illustrating the microstructure of Cu-20 wt% Nb alloys dropped at different stages during the cooling period are illustrated in Fig. 4. The sample presented in Fig. 4a was quenched from the solid + liquid (S + L) state, and its microstructure is similar to that of Fig. 2e. The microstructure for the other two samples (one supercooled by 200 K and dropped a short time after recalescence shown in Fig. 4b, and the other dropped before recalescence shown in Fig. 4c) were taken at the center of the specimen.

The influence of Nb content on the microstructure of the alloys supercooled to 230 K and dropped before recalescence is presented in Fig. 5. Similar to the previous examples, first to solidify are primary Nb dendrites embedded in a cu-rich interdendritic phase. Elemental microanalysis indicates that the Nb dendrite concentration ranges between 95.2 and 96.3 wt% Nb (same as found for the coarse dendrites solidified while levitating). The dendrite density increases with increasing Nb concentration in the specimen. No evidence of melt separation is observed in these specimens. The dendrite morphology in these supercooled samples was found to depend on the effect of distance from the copper chill (manifesting different cooling rates). A typical example is shown in Fig. 6 for

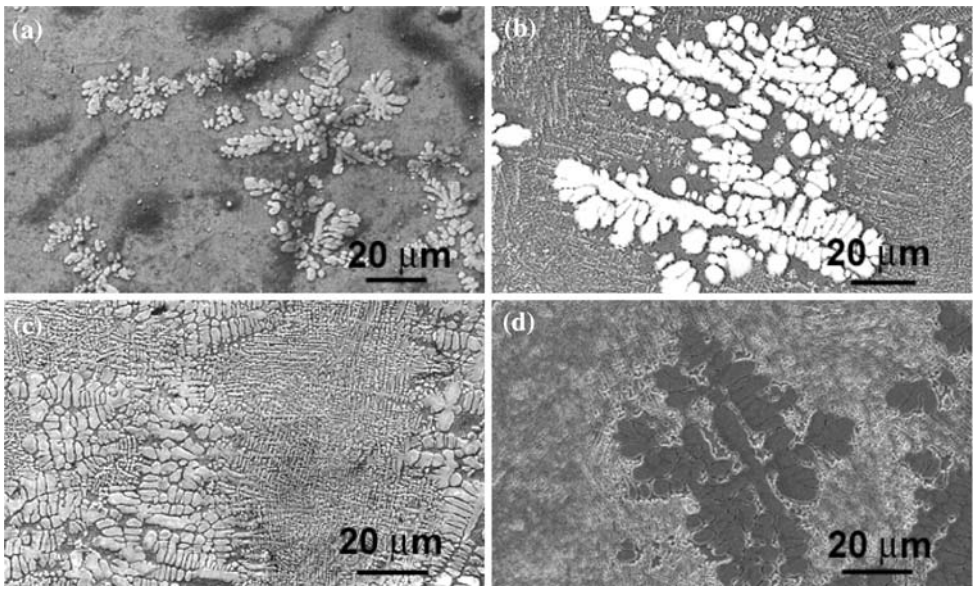

Fig. 2 Secondary electron Images illustrating the microstructure of Cu–Nb alloys dropped from the solid + liquid (S + L) region as a function of Nb concentration in the melt. **a** Cu-5 wt% Nb, **b** Cu-10 wt% Nb, **c** Cu-20 wt% Nb, and **d** Cu- 40 wt% Nb

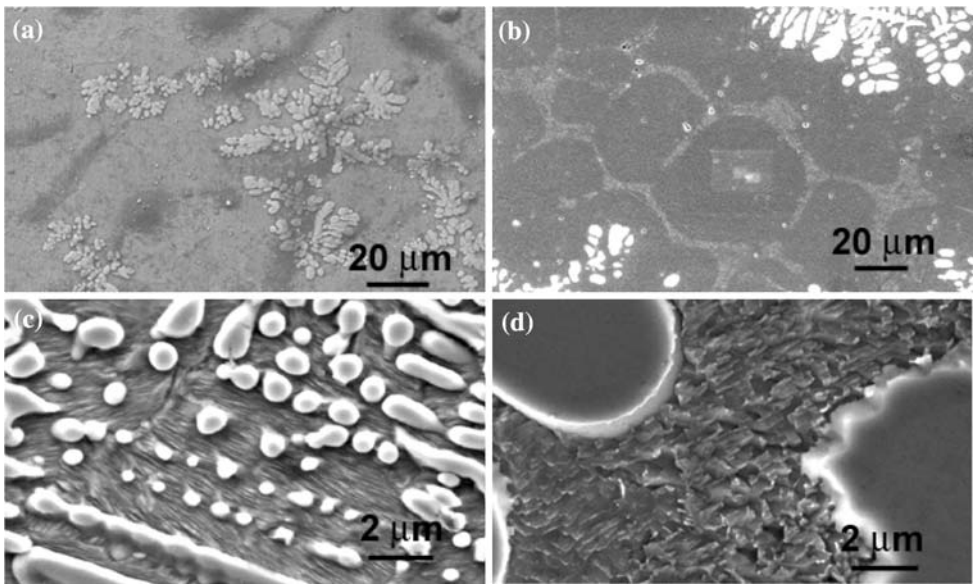

Fig. 3 Secondary electron Images illustrating the impact of Nb concentration on the interdendritic regions in Cu–Nb alloys. **a** Cu-5 wt% Nb; **b** Cu-8 wt% Nb; **c** Cu-20 wt% Nb; **d** Cu-40 wt% Nb

Cu-30 wt% Nb supercooled by 50 K and dropped before recalescence. Up to 100 μm from the copper chill the microstructure consisted of fine columnar cells (Fig. 6a), which gradually changed to regular dendrites farther from the copper chill (about 1200 μm) (Fig. 6c). In between, about 700 μm from the copper chill, a mixed microstructure like that in Fig. 6b was observed.

In contrast with the above mentioned microstructure, a spherical morphology, characteristic of alloys solidifying in the miscibility gap, was observed in Cu–Nb specimens containing 20 wt% Nb, under certain solidification conditions as shown in Fig. 7. When the specimen was supercooled by more than 270 K, and dropped on the copper chill prior to recalescence, the majority of the cross section was composed of these spheres as illustrated in Fig. 7a with some minor fraction of dendrites. The morphology of the spherical elements is illustrated at a higher magnification in Fig. 7b. The spheres comprise of a rim with an interior of dark and bright zones. Elemental microanalysis performed by the SEM indicates that the rim and the bright zones in the center of the spheres contains a higher Nb content while the dark region is rich in Cu. Due to the small dimensions of the phases involved, more accurate determination was obtained using a transmission electron microscope (TEM). In Fig. 8 we present a transmission electron image of a sphere (Fig. 8a) and a dendrite (Fig. 8b) for the Cu-20 wt% Nb supercooled by more than 270 K, and dropped on the copper chill prior to recalescence. Selected area diffraction pattern of zone axis [−131] taken from the sphere rim is superimposed on the bottom

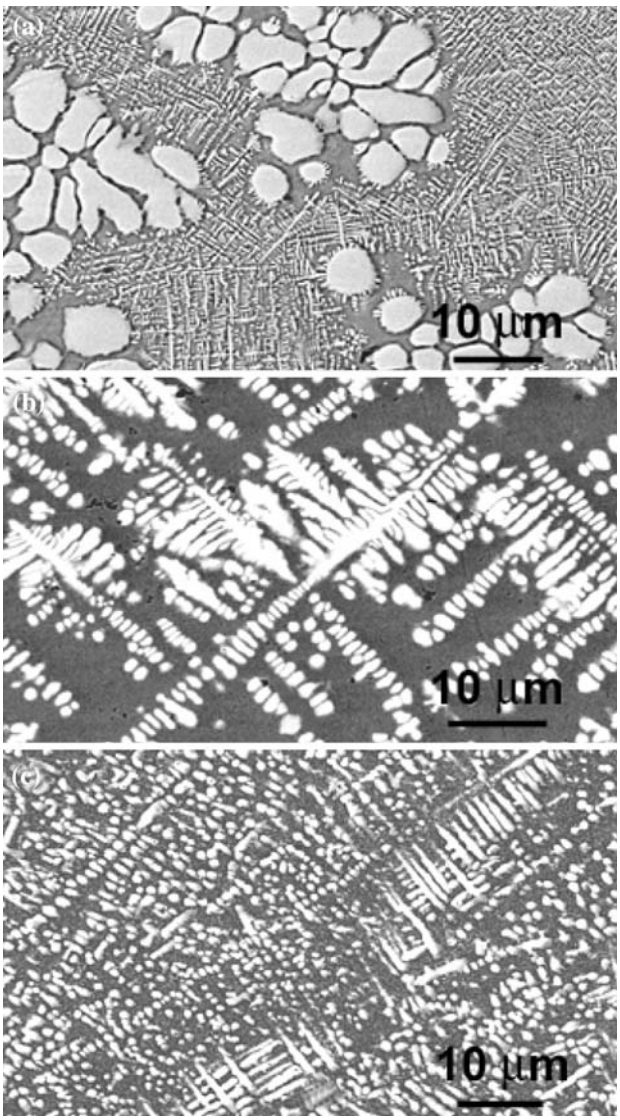

Fig. 4 Secondary electron Images illustrating the microstructure of Cu-20 wt% Nb dropped from different locations on the thermal history. **a** Liquid + solid region; **b** After 200 K supercooling following recalescence; **c** After 200 K supercooling before recalescence

right of the Fig. 8a. For comparison, a bright field image of a dendrite with a selected area diffraction pattern of zone axis [100] is shown Fig. 8b. Both of them (the spherical elements and dendrites) have Nb-bcc lattice parameter. Nevertheless, elemental X-ray analysis indicates that both of them contains only 58–60 at.% Nb (see Table 2) compared to around 98 at.% predicted for a primary Nb dendrite from the stable Nb-Cu phase diagram. In addition, the spherical morphology was also observed in the interdendritic regions of Cu 20 wt% Nb specimens that nucleated while levitating then dropped from the solid + liquid region, Fig. 9. In such cases, as was described earlier, first to nucleate are the coarse Nb dendrites (white dendrite at the lower right corner of Fig. 9a) which grow at small cooling rates. As the melt touches the copper chill, finer dendrites are formed. In the center of the finer dendrites, spherical elements are observed. The spheres' concentration increases as the distance from the chill increases (Fig. 9b).

Thermodynamic calculation

The calculated equilibrium Cu–Nb phase diagram is presented in Fig. 10. The measured melting temperatures at different concentrations are also shown in the figure. A peritectic reaction in the Cu-rich side, as shown in Fig. 10b, was calculated to be at 1093 °C, with the Cu phase forming at this temperature containing 1.3 wt% Nb. The Nb-rich side has a retrograde solubility, with a maximum calculated solubility of 3.5 wt% Cu in Nb. It should be noted that this value is slightly smaller than the concentration actually found in the experiments (3.9 wt% Nb).

The metastable Cu–Nb phase diagram calculated after suppressing the Cu-fcc and Nb-bcc solid phases is given in Fig. 11 (the dashed line). The results show that two melts—one Cu enriched, the other Nb enriched—coexist, which means melt separation is thermodynamically possible if nucleation of Nb or Cu phases does not take place. Superimposed are the calculated T_0 curve (the curve represents the loci where the Gibbs free energy of the solid is equal to that of the liquid phase), and the experimentally suggested miscibility gap. An actual measured at 270 K supercooling for a specimen containing 20 wt% Nb is also shown by the square point.

Discussion

General

When Cu–Nb-levitated specimens nucleate during the levitated state without supercooling, the first phase that nucleates is coarse Nb dendrites. If at that stage high cooling rates are imposed on the specimen by dropping the semi-liquid onto a copper chill, finer dendrites form which grow on top of the coarse ones as evident in Figs. 2 and 3. When the temperature decreases below the peritectic temperature, T_P, a Cu-rich phase begins to solidify via the peritectic reaction. As the reaction continues, the ε-Cu phase grows around the dendrite until the latter is completely surrounded. At this point, the binary peritectic reaction significantly slows down and the remaining liquid solidifies dendritically as ε-Cu dendrites according to the solidus and liquidus lines of the ε-Cu phase. Because of the reverse slope of the solidus and liquidus lines (i.e. partitioning coefficient larger than 1), the center of the ε-Cu cell

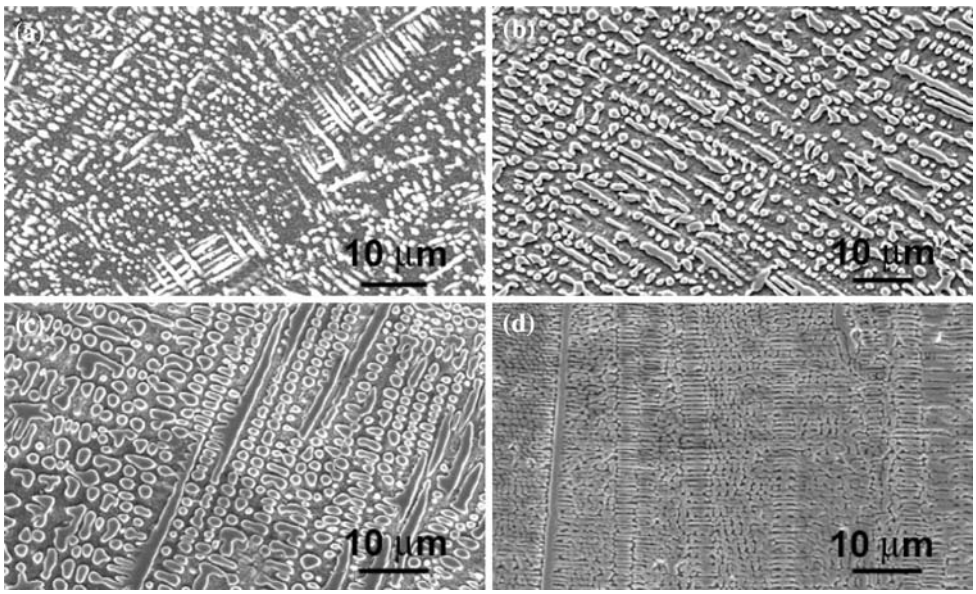

Fig. 5 Secondary electron Images illustrating the microstructure of Cu–Nb alloys supercooled by 230 K, and dropped before recalescence as a function of Nb concentration. **a** Cu-20 wt% Nb; **b** Cu-30 wt% Nb; **c** Cu-40 wt% Nb; **d** Cu-60 wt% Nb

is rich in Nb, containing around 3.9 wt%, while the periphery contains smaller amounts of Nb (around 0.8 wt%). At the cell borders, the Cu concentration is expected to be 100% Cu. However, because the elemental microanalysis performed by the SEM underestimates the true concentration as it is taken from an area with a diameter of about 1–2 μm. The nominal value obtained at the cell border is around 99.2 wt% Cu. The thermodynamic calculation made by us in this study, as well as that of Smith et al. [7], and Chakrabarti and Laughlin [8], indicated that the stable phase diagram of Cu–Nb should exhibit a horizontal liquidus line with a peritectic reaction (Fig. 10).

The type of matrix microstructure shown in Fig. 3a and b is similar to the peritectic microstructure observed in binary Cu–Co [10, 11], Cu–Fe [9] and Cu–Fe–Co [13] systems. The Cu–Co [10, 11] and Cu–Fe [9] stable phase diagrams also exhibit nearly flat liquidus curves. For these systems, the present authors found liquid immiscibility upon supercooling. Therefore, for Cu–Nb system we would expect to find a miscibility gap upon supercooling of the liquid as well. Indeed, thermodynamic calculations performed by suppressing the Cu-fcc and the Nb-bcc solid phases indicate such a miscibility gap, shown by the dashed line in Fig. 11. However, our experimental results indicate that the minimum supercooling required to enter the metastable liquid miscibility gap is much greater than the about 40 °C which the calculation predicts. The minimum supercooling required to enter the miscibility gap for Cu–Nb alloys containing around 20 wt% Nb is 230 K. Our experimental results further show that much higher supercoolings are required to enter the miscibility gap for Cu–Nb alloys containing larger or smaller than 20% Nb. These results confirm the miscibility curve suggested by Smith et al. [7] as shown by dotted curve in Fig. 11 and designated as $T^{\text{exp}}_{\text{misc}}$. The curve is not symmetrical but skewed towards Cu-rich side of the diagram as shown in the dotted line in Fig. 11. The curve shows that the minimum supercooling required to enter the miscibility gap is between 230 and 270 K for Cu-20 wt% Nb alloys. For other Nb concentrations, much higher supercooling is needed, which could not be achieved in our experiments. It is believed that more accurate thermodynamic data is needed for better prediction of the stable and metastable Cu–Nb phase boundaries.

The presence of oxygen impurities, and probably other interstitial elements in the melt might lower the minimum supercooling needed for entering the miscibility gap to values mentioned above. This was suggested by Verhoeven et al. [2] and Smith et al. [7], and established experimentally by Li et al. [17]. The amount of the oxygen in the melt reduces the minimum supercooling required to enter the miscibility gap. The microstructures given in Fig. 9 show that this might indeed be the case when the sample is contaminated with oxygen (as will be discussed at the end of next section).

Phase selection during solidification of supercooled Cu–Nb alloys

In the constructed Cu–Nb phase diagram in Fig. 11, we superimposed the calculated metastable liquid miscibility gap $T^{\text{cal}}_{\text{misc}}$ (dashed line), the experimental suggested liquid miscibility gap $T^{\text{exp}}_{\text{misc}}$ (doted line) [7], and the calculated T_0 curve for Nb. Since there is no meaning of the T_0 curve while entering the miscibility gap [19], we dotted the T_0 curve at that region. There are three distinct regions for nucleation and solidification sequence for the alloys in the cu-rich side of the diagram as described below:

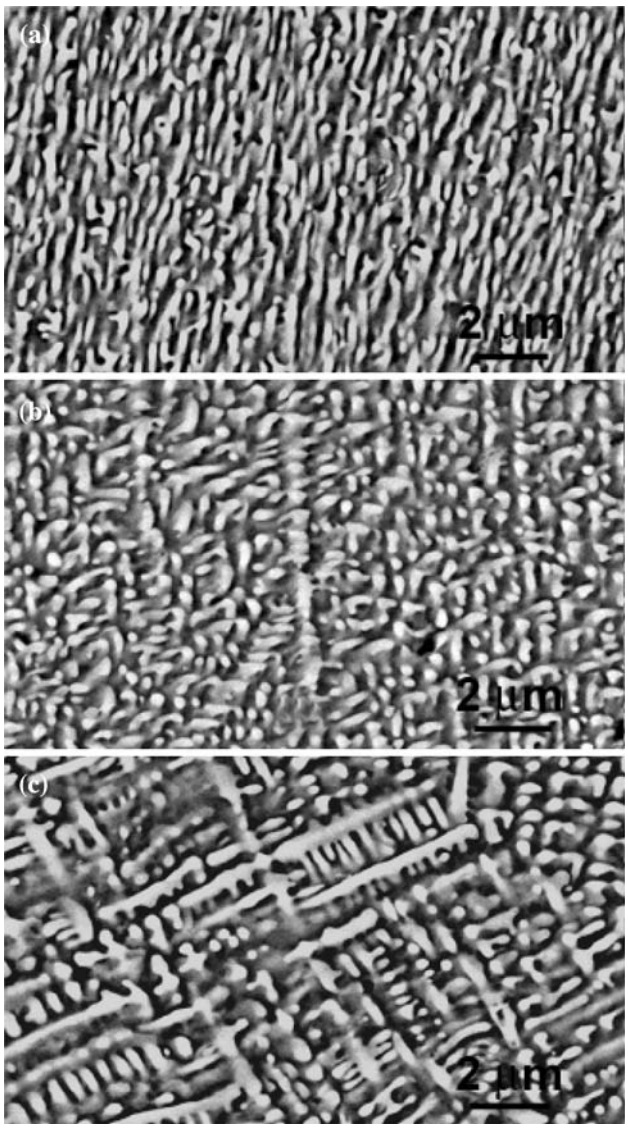

Fig. 6 Secondary electron Images illustrating the microstructure of Cu-30 wt% Nb supercooled at 50 K and dropped before recalescence as a function of distance from the Cu chill. **a** 100 μm from bottom; **b** 700 μm from bottom; **c** 1200 μm from bottom

Nucleation between T_L (liquidus temperature) and T_{misc}

In this case, first to nucleate is the Nb-bcc phase. On cooling, the concentration of the solid and liquid phase will follow the stable phase diagram boundaries. The microstructures shown in Figs. 4 and 5 are representative of such microstructures.

Nucleation between T_{misc} and T_0

In this case, as the liquid enters the immiscibility gap, liquid phase separation takes place. Then, two liquids will form; Nb-rich liquid (L1) and Cu-rich liquid (L2). Each liquid will solidify following the stable phase boundaries.

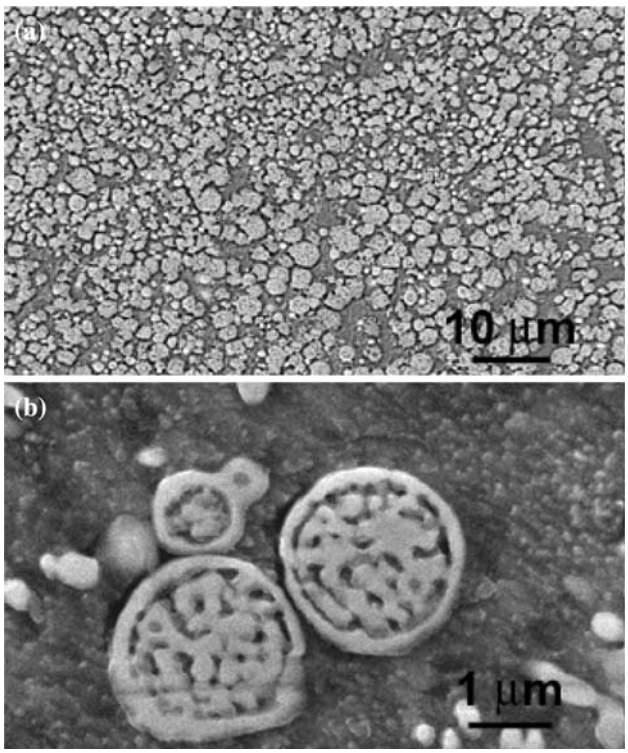

Fig. 7 Secondary electron Images illustrating the formation of Nb spherical morphology in Cu 20 wt% Nb specimen solidified under different conditions. **a** Supercooled by 270 K and dropped before recalescence, at 100-μm distance from the copper chill. **b** Sphere morphology at high magnification

Because the amount of supercooling of the L1 after separation is much higher than that of L2 (see Fig. 11), the L1 liquid will most likely solidify first as spheres. The volume fraction of the spheres will depend on the Nb concentration and the temperature. High cooling rates during solidification could also cause additional dynamic supercooling, or at least keep the liquid in the miscibility gap for a longer time, thus leading to the formation of lager amounts of spheres. It should be noted that at slow cooling rates, the heat released during solidification of the one liquid, say L1, can increase the residual melt temperature above the immiscibility curve, thus causing of remixing of the two melts to form one melt. In such a case, the alloy will solidify following the stable phase boundaries, similar to the microstructure shown in Fig. 9, even though the alloy was supercooled below the miscibility gap.

Nucleation below T_0

In this case, after the liquid enters the immiscibility gap, liquid phase separation takes place. As before, the L1 will solidify first, but because the temperature is below the T_0 curve, the L1 will solidify partitionlessly, with L1 composition. This was actually observed in the TEM result.

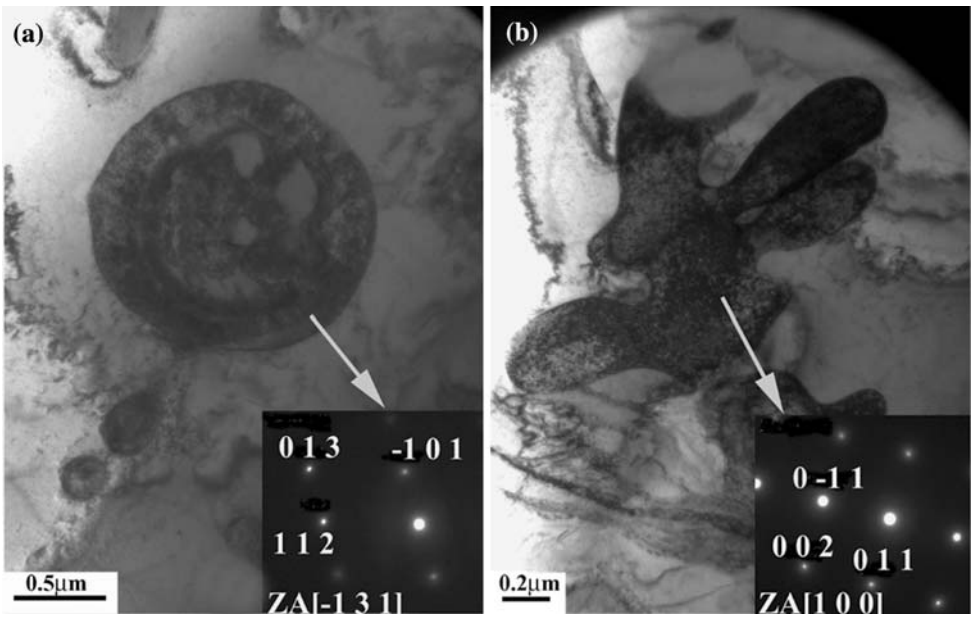

Fig. 8 Transmission electron images of Cu-20 wt% Nb alloy supercooled by 270 K and dropped immediately after recalescence. **a** Bright field image of a sphere. A selected area diffraction pattern of ZA[−131] is superimposed on the bottom right. **b** Bright field image of a dendrite. A selected area diffraction pattern of ZA[100] is superimposed on the bottom right

Table 2 Summary of STEM microanalysis from different areas in Cu-20 wt% Nb supercooled by 270 K and dropped immediately after recalescence

Region	Composition		Composition	
	Cu (wt%)	Nb (wt%)	Cu (at.%)	Nb (at.%)
Matrix outside the sphere	96.1	3.9	97.3	2.7
Bright zone inside the sphere Fig. 8a	96.1	3.9	97.3	2.7
Dark zone inside the sphere Fig. 8a	31.8	68.2	40.5	59.5
Sphere rim	33.3	66.7	42.2	57.8
Dendrite in Fig. 8b	31.8	68.2	40.5	59.5

The sphere's rim and the dark phases inside the sphere (Fig. 8) have a Nb lattice, but with composition of the L1 melt ($\approx$67 wt% Nb) and not that of the regular phase boundary, with about 96 wt% Nb. The particular specimen of Fig. 11 was supercooled by 270 K, and dropped before recalescence. In such a case, usually one obtains a pancake-shaped specimen with small thickness. Therefore, high cooling rates are imposed during the entire solidification path and, the entire cross section experiences melt separation.

Effect of residual oxygen in the Cu–Nb melt on the microstructure

Oxygen has been found to have a strong effect in stabilizing the miscibility gap [7]. Other interstitials, such as carbon and nitrogen, are suspected to have similar effects. Effects of oxygen in causing melt separation were reported by Schelle [20] for Cu–Nb alloys prepared from compressed bars of metal powders using arc melting. The phase separation

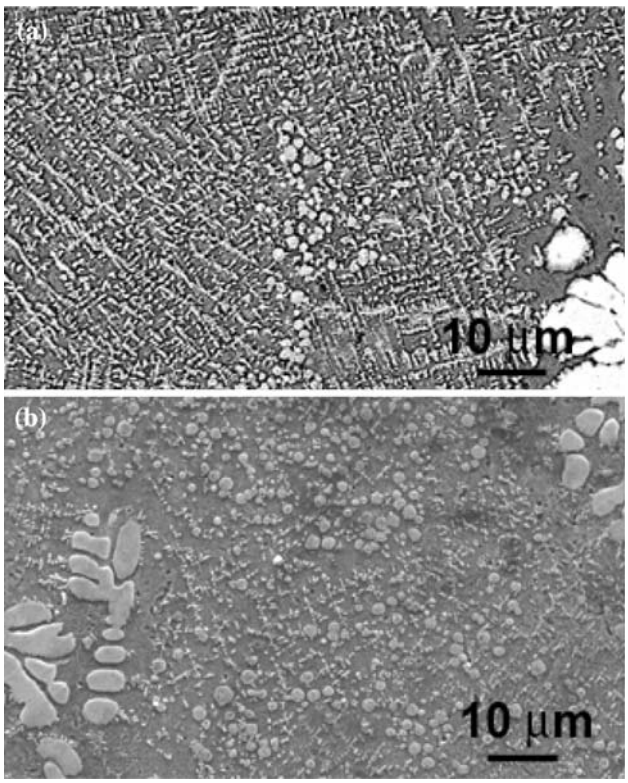

Fig. 9 Secondary electron Images illustrating the formation of Nb spherical morphology in Cu 20 wt% Nb specimens dropped from the solid + liquid region as a function from the Cu chill. **a** 700 μm from the Cu-chill, and **b** 1200 μm from the Cu chill

occurring in alloys of 10–40 wt% Nb was attributed to the relatively high O_2 content in the metal powders. Assuming that large content of O_2 could induce melt separation, the sequence of microstructure evolution present in Fig. 9a and b can be explained as follows: Looking on the micrograph of

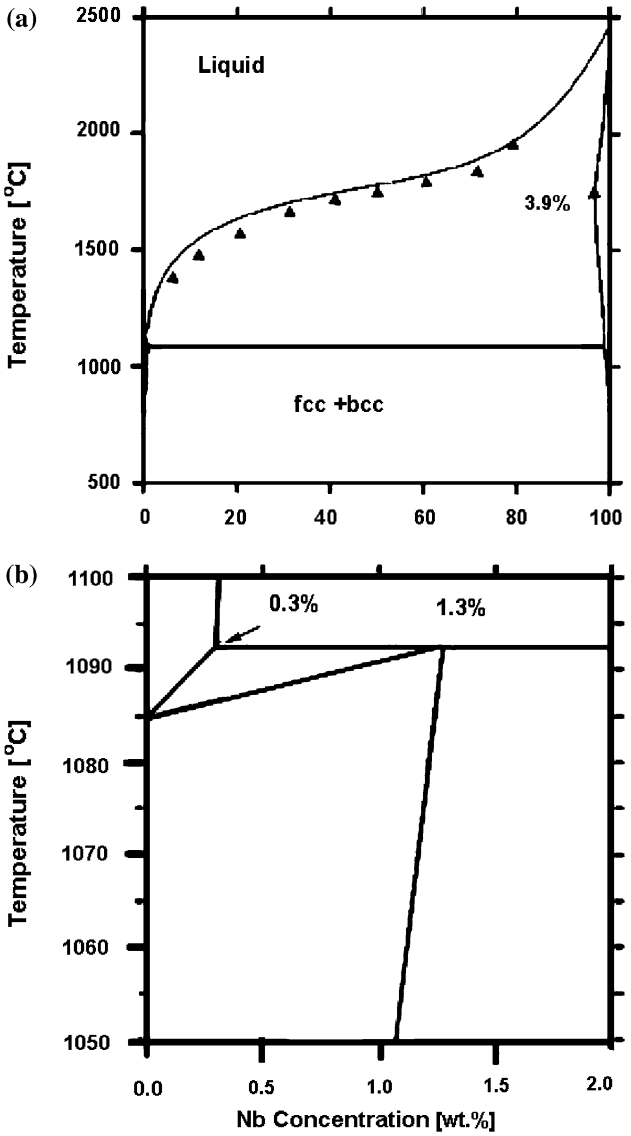

Fig. 10 Calculated Cu–Nb stable phase diagram (**a**), and enlargement of the Cu-rich side (**b**), the phase diagram contains a peritectic reaction at 1093 °C, and the peritectic phase can absorb up to 1.3 wt% Nb. The melting temperature as a function of Nb content found in this study (triangles) and the maximum Cu solubility in Nb are superimposed on the calculated stable Cu–Nb phase diagram

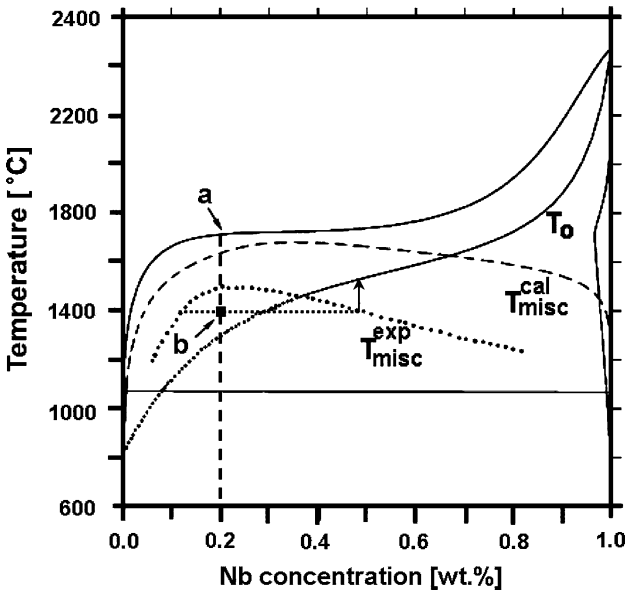

Fig. 11 Calculated metastable liquid miscibility gap T^{cal}_{misc} (dashed line) the experimental suggested liquid miscibility gap T^{exp}_{misc} (doted line), the calculated T_0 curve, are superimposed on the calculated stable phase diagram

Fig. 9b, which was found in numerous specimens, the first to solidify is the coarse Nb dendrite (bright phase at bottom left of the figure). After the specimen is quenched on the copper chill and high cooling rates are imposed, dendritic refinement takes place. Because oxygen present as a minor impurity in the melt is also rejected to the residual melt, its concentration in the melt increases as solidification proceeds. This shifts the T_{misc} upward, bringing it close to the T_L at a composition near to 20 wt% Nb. The high cooling rates imposed due to quenching of the melt on the copper chill maintains the liquid below the shifted miscibility gap; thus, melt separation continues (see next paragraph). In such a case, mixed microstructure of dendrites and spheres, such as in the case shown in Fig. 9b, will be observed. Again, last to solidify is the Cu-fcc phase within the dendrite arms and the spherical particles.

Conclusion: Melt separation may take place for Cu–Nb alloys close to 20 wt% Nb under two opposite conditions, both involving high cooling rates at the end of solidification:

1. *High supercooling level*: In this case, very high supercooling is needed (between 230 and 270 K) which are usually obtained by dropping the specimens before recalescence. The high cooling rates cause two effects: to increase the melt supercooling by additional dynamic supercooling, and to maintain the melt relatively for a longer time in the miscibility region. In such cases, the entire cross section will contain small spheres.
2. *Small supercooling level*: In this case, solidification starts with small cooling rates at the beginning of solidification and enters the solid + liquid (S + L) region and then the sample was quenched onto a copper chill. In such a case, the amount of rejected oxygen will be able to shift the T_{misc} closer to T_L. In such a case, the spheres might nucleate towards the end of the solidification sequence; hence they will be located in the center of the finer dendrites, usually far away from the copper chill (relatively the last melt to solidify).

Usually when melt separation occurs, the L1 liquid solidifies first as spheres because of the higher supercooling

obtained after separation [10, 11] compared with L2 liquid. The spheres in the Cu–Nb system consisted of a Nb-bcc phase rim filled with a network of Nb-bcc phase, and within the network of almost pure Cu. This is a unique microstructure as compared to the L1 spheres in Cu–Co, and in Cu–Co–Fe systems. In these systems, the spheres consisted of a grained structure for alloys up to 20 wt% Co (or Co + Fe), or a dendritic structure for alloys with higher Co concentrations.

In general, as the cooling rates grow, the solidification time becomes shorter, which induces microstructural refinement. It has been argued [21], that under rapid cooling of the order of 10^5–10^6 K/s, a supercooled liquid may continue to supercool further even in the presence of solid nuclei provided that the heat removal rate exceed the heat of fusion releasing rate [22]. Indeed, Clyne [23] has reported that melt quenched on a copper chill might exhibit 200 K supercooling close to the copper chill, and that the supercooling depends on the distance from the copper chill. These two effects (dynamic supercooling and microstructural refinement) have a central role in refinement, as well as morphologies observed in this investigation. For alloys that entered the miscibility gap prior to nucleation, the high cooling rate will enhance heat absorption, and keep the residual liquid in the miscibility gap. For such a case, the entire cross section will consist of spherical elements. On the other hand, when the specimen is quenched from the solid + liquid region, high cooling rates impose dynamic bulk supercooling, which might bring the residual liquid into the miscibility gap. Melt separation will then occur within the dendrites. Rejection of oxygen impurity to the remaining liquid may also raise the miscibility curves, thus enhancing melt separation.

Summary

Electromagnetic levitation was used to study supercooling effects on solidification characteristics of Cu–Nb alloys containing 5–70 wt% Nb. The experimental results, as well as thermodynamic calculations, indicate that the Cu–Nb stable phase diagram exhibits near flat plateau with peritectic reaction at 1080 °C. Melt separation was found only for specimens containing about 20 wt% Nb. The suggested dome-shaped miscibility gap, with a maximum at about 20 wt% Nb in the literature was adopted. We suggest that the amount of oxygen in the melt will determine the minimum supercooling needed to bring the melt into the miscibility gap. The minimum supercooling reduces with increasing oxygen content in the residual melt. When supercooling exceeded 230 K prior to nucleation, combined with high cooling rates, the entire cross section consisted of small spheres, characteristic of alloys that solidify in the miscibility gap under rapid cooling conditions. However, when specimens quenched from the solid + liquid zone on a copper chill, the first to nucleate are the coarse Nb dendrites, followed by the fine dendrites that grow on top of the coarse dendrites. Then, melt separation took place due to the oxygen rejection into the residual melt. Therefore, small spherulites will solidify within the small dendrites.

If the L1 liquid nucleates below the T_0 curve, metastable sphere with Nb-bcc lattice will nucleate containing only 67 wt% Nb as compared to 96 wt% of the regular phase boundary. Because the L1 spherulites solidify a supercooled liquid the sphere rim is the first to solidify and the sphere interior will solidify last in a unique way i.e., a network of Nb-bcc phase and within the network of almost pure Cu filling the holes.

References

1. Zeik KL, Koss DA, Anderson IE, Howell PR (1992) Metall Trans A 23A:2159
2. Verhoeven JD, Gibson ED (1978) J Mater Sci 13:1576. doi:10.1007/BF00553214
3. Frommeyer G, Wassermann G (1975) Acta Metall 23:1353
4. Bevek J, Harbison JP, Bell JL (1978) J Appl Phys 49:6031
5. Popov IA, Shiryaeva NV (1961) Russ J Inorg Chem 6:1184
6. Allibert C, Driole J, Bonnier E (1969) Acad Sci Paris 268C:1579
7. Smith JF, Lee KJ, Baily DM (1984) Bull Alloy Phase Diagrams 5:1984
8. Chakrabarti, Laughlin (1982) Bull Alloy Phase Diagrams 2:455
9. Elder SP, Munitz A, Abbaschian R (1989) Mater Sci Forum 50:137
10. Munitz A, Elder S, Abbaschian GJ (1992) Metall Trans A 23A:1817
11. Munitz A, Abbaschian R (1996) Metall Mater Trans A 27:4049
12. Munitz A, Abbachian R, Cotler C, Shacham C (1996) J High Temp Mater Proc 15:187
13. Munitz A, Bamberger M, Wannaparhun S, Abbaschian R (2006) J Mater Sci 41:2749. doi:10.1007/s10853-006-5598-8
14. Munitz A, Abbaschian GJ, Talyanker M (1991) J Mater Sci 26:5195. doi:10.1007/BF01143213
15. Munitz A, Abbaschian R (1986) In: Koch CC, Collings EW (eds) Undercooled alloy phases. The Metallurgical Society of AIME, New Orleans, Louisiana, March 2–6, p 23
16. Abbaschian GJ, Flemings MC (1983) Metall Trans A 14A:1147
17. Li D, Robinson MB, Rathz TJ, Williams G (1998) Acta Mater 46:3849
18. Kaufman L (1978) Calphad 2:117
19. Baker JC, Cahn JW (1971) In: Solidification-papers presented at a seminar of the American Society for Metals, Oct 11–12, 1969, Metals Park, OH
20. Schelle RF (1971) MSc Thesis, Iowa state
21. Munitz A, Abbaschian R (1998) Metall Trans A 33:3639
22. Mondolfo LF (1982) Grain refinement in casting and welds. In: Abbaschian R, David SA (eds) TMS-AIME Warrendale, PA, p 3
23. Clyne TW (1983) Metall Trans B 15B:369